

Quantum flutter versus Bloch oscillations in one-dimensional quantum liquids out of equilibrium

Michael Knap,^{1,2,3,*} Charles J. M. Mathy,^{2,1,*} Mikhail B. Zvonarev,^{4,5} and Eugene Demler¹

¹*Department of Physics, Harvard University, Cambridge, MA 02138, USA*

²*ITAMP, Harvard-Smithsonian Center for Astrophysics, Cambridge, MA 02138, USA*

³*Institute of Theoretical and Computational Physics,*

Graz University of Technology, 8010 Graz, Austria

⁴*Univ Paris-Sud, Laboratoire LPTMS, UMR8626, Orsay, F-91405, France*

⁵*CNRS, Orsay, F-91405, France*

(Dated: March 18, 2013)

We study the dynamics of an impurity of finite mass injected into a one-dimensional quantum liquid at zero temperature, either at finite velocity or at zero velocity with a force driving the impurity. We obtain accurate results using numerical simulations based on matrix product states, and find that in both cases, the impurity undergoes oscillations, however the physical mechanism is different: the driven impurity undergoes Bloch oscillations by following the ground state branch while continuously emitting phonons, whereas the undriven impurity undergoes coherent quantum oscillations at an emergent energy scale, called quantum flutter in previous work, whose amplitude grows with increasing initial velocity. We find these results to be independent of whether the system is integrable or not, and robust to changes in the microscopics of the model, suggesting that they are universal.

I. INTRODUCTION

Experiments in ultracold atomic systems have recently realized different incarnations of a quantum impurity problem in which, starting from a 1D gas of particles with the same internal state called the background gas, a single particle called the impurity is promoted to a different internal state and its properties over time are studied [1–5]. The background itself exhibits behavior special to one-dimensional quantum systems [6, 7]. Investigations of mobile impurities in such systems contributed to the understanding of various phenomena in 1D many-body physics: excitation spectrum and effective mass [8–11], orthogonality catastrophe [12, 13], logarithmic diffusion of Green’s functions [14, 15], persistence of threshold singularity in spectral functions [16, 17] and its momentum-dependent power-law scaling [14, 18–22], and response to an external driving force [23–27] and external confinement [28–30].

Recently it was shown that if an impurity, initialized in a plane wave with a finite momentum Q , is added to a gas of free fermions (or bosons interacting with each other through infinitely strong δ -function potential) the impurity only sheds a part of its momentum to the background gas and forms a correlated state that no longer decays [31]. Furthermore, if Q is of the order of or larger than the Fermi momentum k_F the momentum of the impurity undergoes coherent oscillations which were called quantum flutter and claimed to be due to the impurity forming a coherent superposition of families of quasi-equilibrium states called polaron-like and exciton-like. These phenomena were demonstrated by examining the

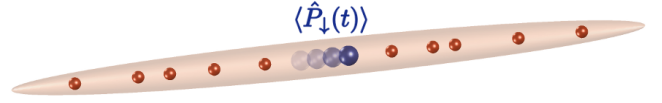


FIG. 1. **Schematic picture of the setup:** (Color on-line) An impurity atom, blue sphere, moves with momentum $\langle \hat{P}_\downarrow(t) \rangle$ through an interacting bosonic background gas initially in its ground state, red spheres. The impurity is injected either in a plane wave with momentum $\langle \hat{P}_\downarrow(0) \rangle = Q$ or at zero momentum with a constant force of strength ϵ_a driving it. The impurity interacts with the background particles through a contact interaction of strength γ , and the background particles interact with each other with a contact interaction of strength γ_{bg} .

full quantum-mechanical evolution obtained from the exact Bethe Ansatz solution which exploits the integrability of the system. Integrability implies the existence of an extensive number of mutually commuting integrals of motion [32, 33]. Thus integrability may largely constraint the dynamics of a system, which poses the question how universal the results obtained for exactly solvable models are. As a general rule, the low-energy dynamics of 1D gapless quantum systems is universal and does not differentiate integrable and non-integrable systems [6, 7], while the equilibration after a strong perturbation reveals a vast amount of integrability-specific phenomena [34–36]. Stemming from a far-out-of-equilibrium initial configuration, quantum flutter is a natural candidate to be tested against various integrability breaking conditions, as we do in this work.

Since the undriven impurity undergoes dissipationless motion, one question which naturally arises is what the effect is of a driving force acting only on the impurity. A semiclassical analysis [27] predicted that the system

* M. Knap and C.J.M Mathy contributed equally to this work.

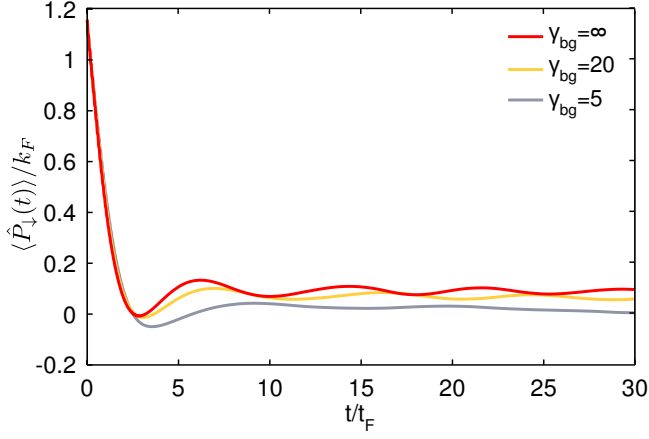


FIG. 2. **Quantum flutter:** (Color online) An impurity (down spin) injected in a plane wave with momentum Q into the background gas (up spins) initially slows down, however, it never comes to a full stop. Further, the impurity momentum $\langle \hat{P}_\downarrow(t) \rangle$ undergoes oscillations in time with an amplitude that grows with increasing initial momentum Q —a phenomenon known as *quantum flutter*, whose full solution for the integrable case of an infinitely repulsive background gas has been explored in Ref. [31]. In this work, we demonstrate that quantum flutter is not specific to integrable systems and robust to changes in the microscopic model. As an example this figure shows quantum flutter in the impurity momentum for a background gas with finite interactions γ_{bg} thus breaking integrability. Units: the background gas has density ρ_\uparrow which defines the Fermi momentum $k_F = \pi\rho_\uparrow$. Momentum is given in units of k_F , and times in units of the Fermi time $t_F = 2m_\uparrow/k_F^2$ where m_\uparrow is the mass of the background particles. Here the masses are considered to be equal: $m_\uparrow = m_\downarrow$.

would reach a finite drift velocity and undergo Bloch oscillations around this velocity. Intuitively, the physical picture is that the impurity is constantly emitting phonons in the background gas and following the ground state branch, which is generically periodic in momentum space for one-dimensional systems, thus leading to periodic effects in the dynamics. The semiclassical analysis assumes that the impurity has a well defined position as a function of time, which implies that the wavefunction of the system can be written as a product of wavefunctions for the impurity and for the background gas. This ansatz should be accurate for heavy impurities, however, for impurities of mass around that of the background particles assessing the validity of that assumption requires an accurate simulation of the time evolution of the system.

In the present paper we present essentially exact results for the dynamics of an impurity injected into a 1D quantum gas by employing the time-evolving block decimation (TEBD) algorithm [37, 38]. First, we show that quantum flutter is not restricted to integrable systems and is robust to changes in the microscopics of the model (see Fig. 2 for representative results). Second, we investigate the effects of a finite force acting on the impurity and find oscillations in the impurity momentum which decay in time and oscillate at a frequency higher than

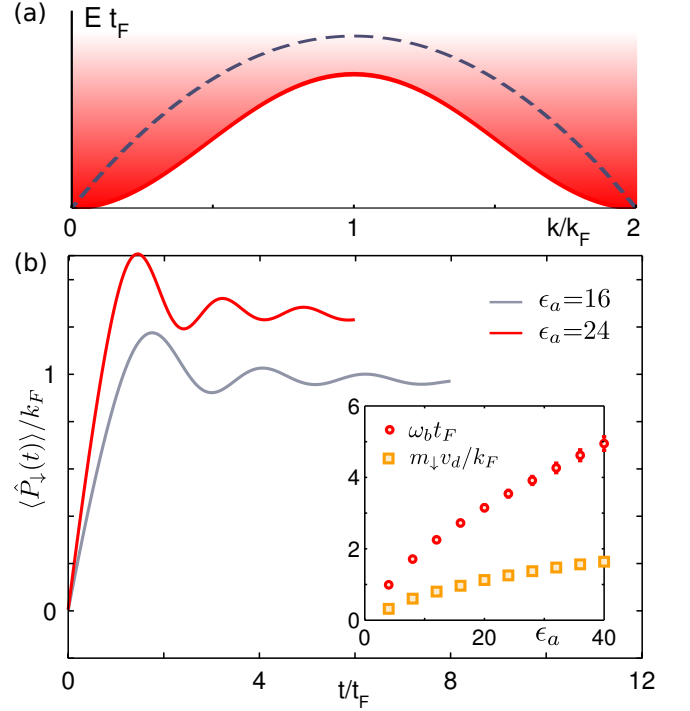


FIG. 3. **Bloch oscillations:** (Color online) (a) Schematic dispersion relation of a repulsive impurity in a background gas, lower solid curve, above which a continuum of manybody excitations exists, that are composed of the moving impurity dressed by a certain number of phonons. For comparison the schematic dispersion of the background gas is shown as well, upper dashed curve, which is linear at low momentum. A force, which acts adiabatically on the impurity, would drive it through the ground state branch leading to Bloch oscillations with period $2k_F$ without energy transfer to the background gas. In contrary, for a finite force the acceleration of the impurity is accompanied with the radiation of phonons, which effectively heats up the system and gives rise to a finite drift velocity around which the impurity performs Bloch oscillations [27]. (b) shows exemplary curves for the impurity momentum as a function of time for two different values of the force ϵ_a confirming the picture of (a). Furthermore, the amplitude of Bloch oscillations around the drift velocity is damped due to nonlinear effects. A stronger force ϵ_a gives rise to an increasing drift velocity v_d as well as an increasing oscillation frequency ω_b , as shown in the inset. For details see main text.

predicted on the basis of a semiclassical analysis [27], see Fig. 3. We compare our results with the experimental results from Ref. [1] which explores such a situation and find that they are quantitatively consistent. We also explore the evolution of the background density around the impurity and find signatures of the driven impurity problem which could also be studied in experiments.

This paper is organized as follows: In Sec. II we present the model at study and discuss details on the numerical method. Results in the absence of a driving force are discussed in Sec. III, where we show that experimentally relevant integrability breaking terms do not affect the

qualitative features of quantum flutter. In Sec. IV we discuss the emergence of Bloch oscillations for an impurity which is driven by a constant force. Finally, we conclude our findings in Sec. V.

II. THE MODEL

In the model we consider a quantum particle (impurity) embedded into a gas of quantum particles of other type (background gas), see schematic illustration in Fig. 1. The motion of the impurity and of the background gas is confined to one spatial dimension. We perform the numerical calculations using a lattice model with a finite number of sites N_s . The system is always studied at low filling, so that the obtained results are representative for the continuum. The Hamiltonian of the model reads

$$\hat{H} = \hat{H}_\uparrow + \hat{H}_\downarrow + \hat{H}_{\downarrow\uparrow}, \quad (1)$$

where

$$\hat{H}_\uparrow = -J_\uparrow \sum_{i=1}^{N_s} (c_{i\uparrow}^\dagger c_{i+1\uparrow} + \text{H.c.}) + \frac{U_{\uparrow\uparrow}}{2} \sum_{i=1}^{N_s} \hat{\rho}_{i\uparrow} (\hat{\rho}_{i\uparrow} - 1) \quad (2)$$

describes the background gas,

$$\hat{H}_\downarrow = -J_\downarrow \sum_{i=1}^{N_s} (c_{i\downarrow}^\dagger c_{i+1\downarrow} + \text{H.c.}) - F \sum_{i=1}^{N_s} x_i \hat{\rho}_{i\downarrow} \quad (3)$$

describes the impurity, and

$$\hat{H}_{\downarrow\uparrow} = U_{\downarrow\uparrow} \sum_{i=1}^{N_s} \hat{\rho}_{i\downarrow} \hat{\rho}_{i\uparrow} \quad (4)$$

describes the interaction of the impurity and background gas. Here $c_{i\sigma}^\dagger$, $c_{i\sigma}$, and $\hat{\rho}_{i\sigma} = c_{i\sigma}^\dagger c_{i\sigma}$ are the creation, annihilation, and the particle number operators on the i th lattice site, respectively. The subscript $\sigma = \uparrow, \downarrow$; we call the impurity a spin-down particle and the particles in the background gas spin-up particles. There is only one impurity in the system, and the number of the background gas particles, N , is arbitrary,

$$\sum_{i=1}^{N_s} \rho_{i\downarrow} = 1, \quad \sum_{i=1}^{N_s} \rho_{i\uparrow} = N. \quad (5)$$

The parameter $U_{\uparrow\uparrow}$ ($U_{\downarrow\uparrow}$) characterizes the on-site repulsion energy between two background particles (background particle and impurity); J_σ specifies the hopping energy. The last term on the right hand side of Eq. (3) describes a constant force F applied to the impurity, $x_i = ia$ being the position of i th site and a the lattice spacing. The background particles satisfy bosonic statistics: the operators $c_{i\uparrow}^\dagger$ and $c_{i\uparrow}$ have canonical commutation relations, $[c_{i\uparrow}^\dagger, c_{j\uparrow}] = \delta_{ij}$. Thus, the model (1) is a particular case of the spin-1/2 Bose-Hubbard model (Eq. (5) restricts the number of spin-down particles to one).

We denote the ground state of the background gas, Eq. (2), as $|\text{BG}\rangle$. We then initialize the impurity in a plane wave with momentum Q :

$$|\psi(t=0)\rangle = c_{Q\downarrow}^\dagger |\text{BG}\rangle, \quad (6)$$

where the operator $c_{Q\downarrow}^\dagger = \frac{1}{\sqrt{N_s}} \sum_{j=1}^{N_s} e^{iQx_j} c_{j\downarrow}^\dagger$ creates an impurity with momentum Q . In our numerical simulations the state $|\psi(t)\rangle = e^{-i\hat{H}t} |\psi(t=0)\rangle$ is represented as a matrix product state (MPS). We start with determining the initial ground state $|\text{BG}\rangle$ by density matrix renormalization group [39, 40], and then add the impurity as given by Eq. (6). Subsequently, we evolve the system in time using the time-evolving block decimation (TEBD) algorithm [37, 38]. We push TEBD to perform high-accuracy simulations: Specifically, the presented results are obtained for systems with $N_s = 400$ lattice sites, $N = 40$ particles, and MPS bond dimension $M = 400$ or $M = 500$, which determines the numerical accuracy of the calculations. In Fig. 4, we consider even a double as large MPS bond dimension $M = 800$, which increases the numerical effort by a factor of eight, and in Fig. 5 we increased the simulated systems to $N_s = 600$, $N = 60$, and $M = 600$. We verified that all the results are representative for the continuum and when appropriately rescaled, see below, do *not* depend on N , N_s and on the MPS bond dimension M .

We are aiming our numerics at the analysis of the continuum limit of the model defined by Eq. (1)–(5). The limit is taken as usual (see, for example, Chapter 2 of Ref. [41]). Namely, $c_{j\sigma} \rightarrow \sqrt{a} \Psi_\sigma(x)$, where $x = aj$. The density operator in the continuum $\hat{\rho}_\sigma(x) = \Psi_\sigma^\dagger(x) \Psi_\sigma(x)$. The summation over lattice sites is replaced with the integration, $\sum_{j=1}^{N_s} a f(aj) \rightarrow \int_0^L dx f(x)$, where f is an arbitrary function, and $L = N_s a$. Thus,

$$-J_\sigma \sum_{j=1}^{N_s} (c_{j\sigma}^\dagger c_{j+1\sigma} + \text{H.c.}) \rightarrow \frac{\hat{P}_\sigma^2}{2m_\sigma}, \quad \sigma = \uparrow, \downarrow, \quad (7)$$

where $m_\sigma = 1/(2J_\sigma a^2)$ and

$$\hat{P}_\sigma^2 = - \int_0^L dx \Psi_\sigma^\dagger(x) \partial_x^2 \Psi_\sigma(x). \quad (8)$$

The impurity-background interaction term, Eq. (4), takes the form

$$\hat{H}_{\downarrow\uparrow} = g \int_0^L dx \hat{\rho}_\downarrow(x) \hat{\rho}_\uparrow(x), \quad g = a U_{\downarrow\uparrow}. \quad (9)$$

It is convenient to use the dimensionless parameter γ for the strength of the impurity-background interaction:

$$\gamma = \frac{m_\uparrow g}{\rho_\uparrow} = \frac{U_{\downarrow\uparrow}}{2J_\uparrow n_\uparrow}, \quad (10)$$

Here we used that $\rho_\uparrow = N/L$ and $n_\uparrow = N/N_s$. The continuum limit of the interaction term in Eq. (2) is

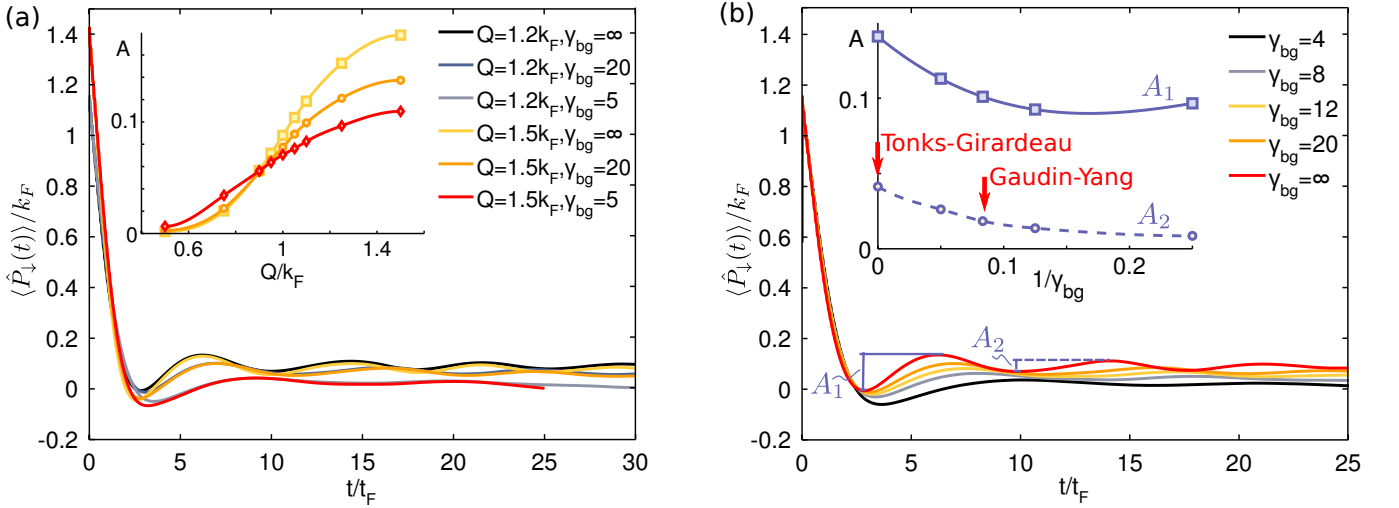


FIG. 4. **Impurity momentum as a function of time:** (Color online) An impurity with momentum Q is immersed in a one-dimensional interacting bosonic liquid. The expected impurity momentum $\langle \hat{P}_\downarrow(t) \rangle$ is plotted as a function of time. $\langle \hat{P}_\downarrow(t) \rangle$ first decays to finite value, and then oscillates as a function of time. The simulations are carried out using TEBD on a spin-1/2 Bose-Hubbard model that is dilute enough to obtain results that are valid for the continuum limit. The interaction between the impurity and background particles is fixed at $\gamma = 12$. The simulations have converged and do not depend on number of lattice sites N_s , number of particles N or MPS bond dimension M (the largest system we simulated had $N_s = 400$, $N = 40$ and $M = 800$. N/N_s must remain small enough to avoid lattice effects, we found the results to be independent of N as long as $N/N_s < 0.2$). (a) Time evolution of $\langle \hat{P}_\downarrow(t) \rangle$ for a set of different initial momenta and background interaction strengths γ_{bg} . After the initial decay, the plots depend weakly on the initial momentum Q , provided Q is large compared to k_F . Inset: quantum flutter amplitude A as a function of initial momentum, where the amplitude is defined as the difference in $\langle \hat{P}_\downarrow(t) \rangle$ between the first maximum and first minimum. The amplitude grows with Q , and the second derivative of A as a function of Q changes sign at $Q = k_F$. The growth in A is increasingly sharp as γ_{bg} increases, in other words as the system becomes more fermionic (at $\gamma_{bg} = \infty$ the system is fermionizable). Colors indicate γ_{bg} as in the main figure. (b) A closer look at the dependence on γ_{bg} . Plotted is $\langle \hat{P}_\downarrow(t) \rangle$ for $\gamma = 12$ and for $\gamma_{bg} = 4, 8, 12, 20, \infty$ from bottom to top. The limits $\gamma_{bg} = \infty$ and $\gamma_{bg} = \gamma$ are both integrable, the former via fermionization, the latter being the Gaudin-Yang model. Inset: amplitude as a function of γ_{bg} . The solid line, labeled A_1 , is defined as in the inset of (a), and initially decays with decreasing γ_{bg} but finally increases again for small enough γ_{bg} , where one sees a pronounced revival of momentum which then reaches a maximum and finally decays to zero while oscillating with negligible amplitude. The first minimum and maximum are therefore special, as the system is still forming the correlation hole around the repulsively interacting impurity and only settles into quantum flutter afterwards. Thus a possibly more meaningful definition of quantum flutter amplitude is given by the dashed line, labeled A_2 , which shows the difference in $\langle \hat{P}_\downarrow(t) \rangle$ between the second minimum and second maximum. This quantity strictly decreases with decreasing γ_{bg} . This indicates that the oscillations are strongest in the fermionic limit. See also the main panel for a graphical illustration of the definition of the amplitudes A_1 and A_2 .

$\frac{g_{bg}}{2} \int_0^L dx \hat{\rho}_\downarrow(x) \hat{\rho}_\uparrow(x)$ and the dimensionless interaction strength between the background particles is

$$\gamma_{bg} = \frac{m_\uparrow g_{bg}}{\rho_\uparrow} = \frac{U_{\uparrow\uparrow}}{2J_\uparrow n_\uparrow}. \quad (11)$$

The model we consider is exactly solvable for some particular values of parameters (as mentioned in the Introduction, we interpret the model to be integrable for those values of parameters): A necessary condition for the integrability is $J_\uparrow = J_\downarrow$. When $F \neq 0$ the model (1)–(5) (and its continuum limit) admits exact solution for $U_{\uparrow\uparrow} = U_{\downarrow\downarrow} = +\infty$ only. Letting $F = 0$ makes the model (1)–(5) exactly solvable for $U_{\uparrow\uparrow} = \infty$ and arbitrary $U_{\downarrow\downarrow}$, where it can be mapped onto a model of fermions interacting with a single particle of other type. That mapping was used, in particular, in Ref. [31]. When $U_{\uparrow\uparrow} = U_{\downarrow\downarrow} \neq \infty$ the model (1)–(5) is not integrable, how-

ever, its continuum limit is integrable: it is known as the Gaudin-Yang model [42, 43]. For any other choices of the parameters the model is, most probably, not integrable.

III. DYNAMICS IN THE ABSENCE OF A DRIVING FORCE

We consider the case without a force $F = 0$ and the impurity initialized in a plane wave with finite momentum Q on top of the background liquid in Fig. 4. We assume equal masses $m_\downarrow = m_\uparrow$, unless mentioned otherwise. We track the expected impurity momentum $\langle \hat{P}_\downarrow(t) \rangle$ as a function of time, where $\hat{P}_\downarrow = \sum_k k c_{k\downarrow}^\dagger c_{k\downarrow}$. We define the operator $\hat{T}_i = c_{i+1\downarrow}^\dagger c_{i\downarrow} - c_{i\downarrow}^\dagger c_{i+1\downarrow}$. If the system were translationally invariant, one could use the fact that $\sum_i \hat{T}_i = -\sum_k 2i \sin(ka) c_{k\downarrow}^\dagger c_{k\downarrow}$, which in the limit $a \rightarrow 0$

becomes $-2ia\hat{P}_\downarrow$, to calculate the impurity momentum. In our simulations open boundary conditions are used, which are not translationally invariant. However, near the center of the trap $\langle\psi(t)|\hat{T}_j|\psi(t)\rangle$ is weakly dependent on the site j at times before finite size effects become important, which occurs once excitations start to reflect off the boundary and arrive at the center of the system. We average $\langle\psi(t)|\hat{T}_j|\psi(t)\rangle$ over the central 20% of the simulated system, and verified that the results did not change with modest change of the size of the area that is being averaged over. From this quantity we can directly use $\langle\hat{P}_\downarrow(t)\rangle = \frac{i}{2a\Delta} \sum_{j=(N_s-\Delta)/2}^{(N_s+\Delta)/2} \langle\psi(t)|\hat{T}_j|\psi(t)\rangle$ with $\Delta = 0.2N_s$ to extract the impurity momentum. In general we find that the momentum does not decay to zero, instead it decays to a finite value. Furthermore, the momentum shows damped oscillations as a function of time whose amplitude grows with increasing initial momentum Q , see inset in Fig. 4 (a), where the amplitude is defined as the difference in $\langle\hat{P}_\downarrow(t)\rangle$ between the first minimum and first maximum. The second derivative of the amplitude as a function of Q is zero at $Q = k_F$. In Fig. 4 (b) we study in more detail the dependence of $\langle\hat{P}_\downarrow(t)\rangle$ on the background gas interaction strength γ_{bg} . Throughout this work we use the Fermi momentum $k_F = \pi\rho_\uparrow$ and the Fermi time $t_F = 2m_\uparrow/k_F^2$ as proper units.

In the case of $\gamma_{bg} = \infty$ it was argued that quantum flutter results from the impurity forming a superposition of two families of quasi-equilibrium states [31], one with the total system (background gas plus impurity) in its lowest energy state at momentum $k = k_F$ and the other with the dressed impurity at zero momentum $k = 0$ and an excitation of the background at $k = k_F$. If the initial momentum $Q > k_F$, any momentum in excess of k_F is sent out in a wave packet. So far the energies of these states have not been calculated except in the limits where the system is integrable [22, 31]. Since in passing we obtain results for the symmetric Gaudin-Yang case $\gamma = \gamma_{bg}$ in this work, we verify that this relationship holds in that limit as well, as we plot in Fig. 5. For the Gaudin-Yang model the ground state of the background plus impurity at finite momentum is known as a magnon, and finite momentum excitations of the background are known as plasmons [14, 22]. Quantum flutter for this bosonic system is due to the dynamical formation of a coherent superposition of a plasmon at k_F and a magnon at k_F , as we describe in more detail below.

The red squares in Fig. 5 (a) denote the frequency of the oscillations in $\langle\hat{P}_\downarrow(t)\rangle$, which we call the quantum flutter frequency $\hbar\omega_f$, extracted from the TEBD simulations. Specifically, we take the set of distances in time from one extremum in $\langle\hat{P}_\downarrow(t)\rangle$ to the next, which each give a value δt for half of the flutter period. The mean of this dataset $\langle\delta t\rangle$ is related to the flutter frequency through $\omega_f = \pi/\langle\delta t\rangle$ shown as red squares and the corresponding error bars are determined from the propagated standard deviation.

The plasmon-magnon gap at k_F is indicated by the

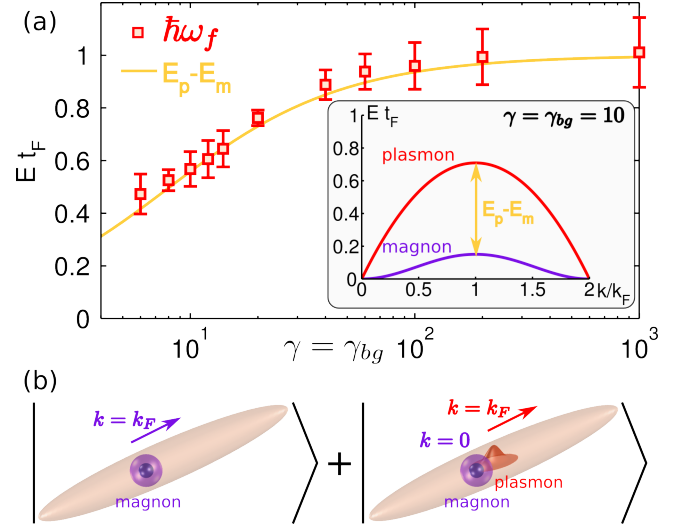


FIG. 5. **Quantum flutter frequency:** (Color online) (a) Comparison of the quantum flutter frequency of oscillations in $\langle\hat{P}_\downarrow(t)\rangle$ with the plasmon-magnon gap for the symmetric model, where $\gamma = \gamma_{bg}$. The red squares denote the quantum flutter frequency ω_f extracted from the TEBD simulations while the solid line corresponds to the plasmon-magnon gap at k_F obtained exactly with Bethe Ansatz [22], which the data agrees with within the error bars. The inset shows the plasmon and magnon dispersions at $\gamma = \gamma_{bg} = 10$. The magnon dispersion is the ground state energy of the system (background gas plus impurity) as a function of total momentum k . The plasmon dispersion gives the minimum energy of particle-hole excitations with total momentum k in the background gas, which is linear for small k [44]. (b) Intuition behind quantum flutter: An impurity injected into the background gas with momentum $Q = k_F$, is in a superposition of a magnon (a dressed impurity) with momentum $k = k_F$, left, and a plasmon (a density excitation of the background gas) with momentum $k = k_F$ while the dressed impurity is at rest $k = 0$, right. Any initial momentum $Q > k_F$ in excess of k_F would be emitted in a wave packet excitation of the background gas.

solid curve which agrees with the flutter frequency to within error bars. Plasmon $E_p(k)$ and magnon $E_m(k)$ dispersions are shown in the inset for $\gamma = \gamma_{bg} = 10$. The magnon dispersion $E_m(k)$ gives the ground state energy of the system (background gas plus impurity) as a function of total momentum k with $E_m(k = 0)$ set to zero. The plasmon dispersion $E_p(k)$ is linear at small momentum [44] and characterizes the lowest energy to create particle-hole excitations in the background gas at finite total momentum k , once again with $E_p(k = 0)$ set to zero. The difference between the plasmon and magnon dispersions at $k = k_F$ is what we call the plasmon-magnon gap.

The interpretation is as follows: if the impurity is injected in the system at momentum $Q = k_F$, it can either form a magnon (a dressed impurity) at momentum k_F or create a dressed impurity with zero momentum and emit a plasmon (an excitation of the background) with

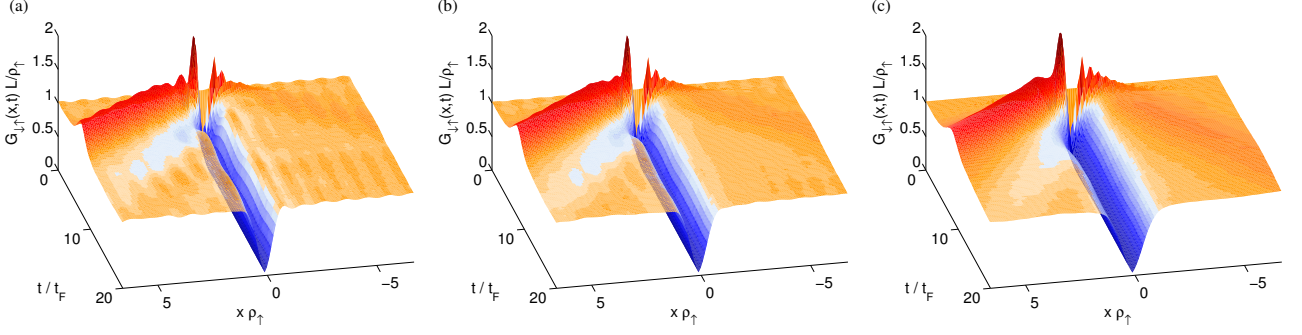


FIG. 6. **Formation of the correlation hole and wave packet emission:** (Color online) Plot of the density-density correlator $G_{\downarrow\uparrow}(x, t) = \langle \hat{\rho}_{\downarrow}(0, t) \hat{\rho}_{\uparrow}(x, t) \rangle$, which corresponds to the density of the background gas around the impurity. Shortly after injecting the impurity a pronounced correlation hole (blue valley) is formed due to the repulsive interactions. This process is accompanied by the emission of a wave packet (red peak) in the background gas that carries away the impurity momentum. The time evolution of the correlations $G_{\downarrow\uparrow}(x, t)$ is shown for $\gamma = 12$, $Q = 1.5k_F$, and (a) $\gamma_{bg} = \infty$, (b) $\gamma_{bg} = 20$, and (c) $\gamma_{bg} = 5$. Other system parameters are the same as in Fig. 4. The qualitative features do not depend on the background interaction. The main changes as γ_{bg} is lowered are the disappearance of the Friedel oscillations in the background, and growth in the size of the correlation hole.

momentum k_F . In Fig. 5 (b) we show the resonant case, where the incoming momentum is precisely enough to create a deep hole. If the impurity is initialized with a momentum Q larger than k_F the excess in momentum is carried away through an emitted wave packet. In the resonant case the total energy of the magnon-like state is $E_{N\uparrow} + E_m(k=0) + E_m(k_F)$ and of the plasmon like state $E_{N\uparrow} + E_m(k=0) + E_p(k_F)$, where $E_{N\uparrow}$ is the total energy of the N background gas particles. Thus the difference between E_1 and E_2 is the plasmon-magnon gap $E_p(k_F) - E_m(k_F)$ which corresponds to the flutter frequency. This strongly suggests that the physics is governed by the formation of a coherent superposition of these two quasi-equilibrium states.

The correlation function

$$G_{\downarrow\uparrow}(x, t) := \langle \hat{\rho}_{\downarrow}(0, t) \hat{\rho}_{\uparrow}(x, t) \rangle \quad (12)$$

measures the background density with respect to the impurity position as a function of time, and shows a pronounced peak which corresponds to the emission of a wave packet that carries away most but not all of the impurity momentum, see Fig. 6. Furthermore the repulsively interacting impurity builds up a correlation hole around itself. These qualitative results do not change as one varies the background interaction strength. The main changes as one goes away from the Tonks-Girardeau (TG) limit $\gamma_{bg} = \infty$ are that the Friedel oscillations disappear and that the width of the correlation hole increases. Note that whereas in [31] Friedel oscillations appeared after a finite time, as a consequence of the formed correlation hole which breaks translational invariance, their presence here at all times is quite natural, because of open boundary conditions used in the numerical simulations. In particular, when moving away from the boundary, Friedel oscillations decay as $\cos(k_F x) x^{-2K}$, where K is the Luttinger parameter [6, 7], giving rise to a faster

decay with increasing K , which is in agreement with the results in Fig. 6.

Changing the mass of the impurity with respect to the mass of the background particles, which makes the system nonintegrable, does not affect the qualitative results, see Fig. 7. We find that the impurity momentum $\langle \hat{P}_{\downarrow}(t) \rangle$ exhibits quantum flutter also in that limit provided the ratio of the masses does not get too large or too small. Empirically, we find that for $0.5 \lesssim m_{\downarrow}/m_{\uparrow} \lesssim 2.0$ quantum flutter is still pronounced, see Fig. 7. In the inset of this figure we show the amplitude of the oscillations where, as in Fig. 4 (b) the solid line corresponds to the amplitude of the first revival of $\langle \hat{P}_{\downarrow}(t) \rangle$, whereas the dashed line indicates the difference in $\langle \hat{P}_{\downarrow}(t) \rangle$ between the second maximum and second minimum. From the latter it turns out that the integrable point $m_{\downarrow} = m_{\uparrow}$ exhibits the strongest quantum flutter oscillations. This is in contrast to the first revival, whose amplitude is shifted toward lighter impurities, which can be attributed to the formation of the correlation hole at short times.

An experimental realization in a cold atomic setup will typically have a harmonic background trapping potential, thus we add to the Hamiltonian:

$$H_T = \sum_{\sigma} \sum_{i=1}^{N_s} \frac{1}{2} m_{\sigma} \omega_T^2 x_{i\sigma}^2 \rho_{i\sigma}, \quad (13)$$

where ω_T is the trapping frequency. The trap breaks translational symmetry, thus momentum is no longer a good quantum number, which begs the question how quantum flutter is affected. In Fig. 8 the impurity momentum is shown in the presence of a trapping potential. The frequency of quantum flutter ω_f increases quadratically with the trap frequency ω_T , see inset of Fig. 8. In this inset, we plot a gray line that corresponds to an equilibrium calculation of an energy which agrees exactly

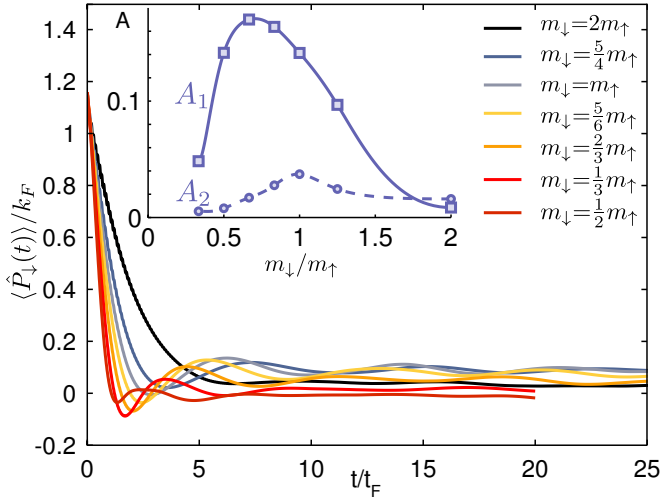


FIG. 7. **Effect of mass imbalance:** (Color online) When the masses $m_\downarrow \neq m_\uparrow$, the model is no longer integrable. This does not change the phenomenology of quantum flutter. In this plot we take the background to be in the TG limit ($\gamma_{bg} = \infty$), the impurity-background coupling $\gamma = 12$, and the initial impurity momentum $Q = 1.2k_F$. Other parameters are as in Fig. 4. Inset: The lines are defined as in the inset of Fig. 4 (b). The amplitude A_2 of the quantum flutter oscillations (dashed line) is strongest for the integrable case of equal masses, whereas the first revival A_1 (solid line) grows for lighter impurities with a maximum at $m_\downarrow/m_\uparrow \sim 2/3$. The shift of the maximum can be attributed to the formation of the correlation hole at short times.

with the quantum flutter frequency. This is analogous to the plasmon-magnon gap discussed above, however we must now find the equivalent quantity for a system with broken translational system.

Quantum flutter is intuitively due to beating between two types of states, magnon-like and plasmon-like, the frequency of which is given by the plasmon-magnon gap. In the TG regime this energy difference can be expressed through absolute ground state energies; quantities which are also meaningful for a system with broken translational symmetry. Specifically, the magnon-like state corresponds to putting the impurity in the lowest unoccupied orbital and fully symmetrizing the spin sector, thus eliminating all interactions. The energy of this state is simply $E_{N\uparrow} + \mu_\uparrow$ since it is equivalent to the ground state with $N+1$ up spin particles and a global spin rotation applied. When the system is translationally invariant this state corresponds to the ground state at momentum k_F . This can be seen by realizing that the minimum kinetic energy of the system, given that the total momentum is k_F , is $E_{N\uparrow} + k_F^2/(2m_\downarrow)$. The Fermi sea of $N+1$ particles, i.e., the state with fully symmetrized spin sector, has this kinetic energy, provided the masses are equal as we consider here, and no interaction energy, therefore it is the ground state at k_F , which is the magnon-like state we were looking for and is a Slater determinant of the lowest $N+1$ orbitals. If we replace plane waves with orbitals

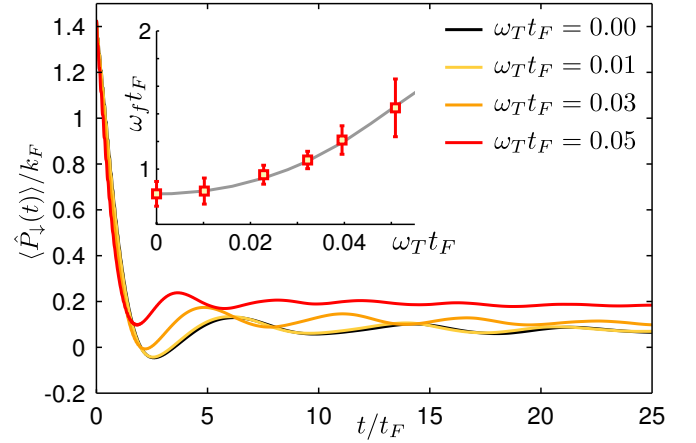


FIG. 8. **Harmonic confinement potential:** (Color online) Quantum flutter in the presence of harmonic confinement with frequency ω_T . The background gas is strongly interacting $\gamma_{bg} = \infty$ and the initial impurity momentum $Q = 1.5k_F$. Other system parameters are chosen as in Fig. 4. The presence of the harmonic trap does not affect the qualitative features, however the flutter frequency grows quadratically with the trapping frequency, see red square in the inset. The gray line in the inset denotes the plasmon-magnon gap extracted using DMRG, see text. Thus quantum flutter frequency once again corresponds to the plasmon-magnon gap.

that are eigenstates of the trapping potential then analogous states can be created: for example, the “Fermi sea” of N particles becomes the occupation of the lowest N eigenstates, which are Hermite functions for a harmonic trap, the background chemical potential becomes the energy of the lowest unoccupied state, and the energy of a deep hole is the energy of the lowest occupied state.

Meanwhile, the plasmon-like state starts with the background of N up spins, takes a particle from the lowest occupied orbital to the lowest unoccupied orbital making a deep hole and adds a dressed impurity in its ground state. The energy of the plasmon-like state consists thus of the following three contributions: (i) the energy of the Fermi sea $E_{N\uparrow}$, (ii) the energy of the lowest unoccupied orbital μ_\uparrow minus the energy of the lowest occupied orbital E_\uparrow^{\min} , and (iii) the dressed impurity chemical potential μ_\downarrow^γ . Now, for equal masses, E_\uparrow^{\min} is also the impurity chemical potential $\mu_\downarrow^{(\gamma=0)}$ when the impurity does not interact with the background, as it will then occupy the lowest orbital. Using this fact we obtain for the energy of the plasmon-like state: $E_{N\uparrow} + \mu_\uparrow - \mu_\downarrow^0 + \mu_\downarrow^\gamma$. Thus the energy difference between plasmon- and magnon-like states becomes $\hbar\omega_f = \mu_\downarrow^\gamma - \mu_\downarrow^0$ and can be calculated with DMRG, which is how we obtain the gray line in Fig. 8.

The dependence of the flutter frequency on the trap frequency is well described by that energy gap. For a background gas consisting of Rb atoms of linear density $\rho = 10^4 \text{cm}^{-1}$ at the trap center, the simulated trapping frequencies correspond to $\omega_T \sim 2\pi \times \{6, 18, 29\}$ Hz (main

figure).

IV. DYNAMICS IN THE PRESENCE OF A CONSTANT DRIVING FORCE

Turning to the case of constant force acting on the impurity, we start the impurity in a plane wave with momentum zero and track its momentum as a function of time. We find that initially the impurity accelerates as though it was free falling and subsequently after a few (roughly two) Fermi times reaches a final velocity v_d (called drift velocity in [27]) around which it performs Bloch oscillations, see Fig. 9 (a). These Bloch oscillations occur due to the $2k_F$ periodicity of the ground state dispersion of interacting one-dimensional systems. Thus they have to be distinguished from Bloch oscillations of free particles on a lattice, where the presence of the lattice itself renders the dispersion 2π periodic. Note that for infinitesimal driving, the impurity would adiabatically follow the ground state branch of the dispersion, and thus not move on average. In contrast for finite driving force the acceleration of the impurity is accompanied with the continuous emission of phonons in the background gas, which in turn leads to the finite drift velocity.

To quantify the acceleration G we introduce its dimensionless pendant as $\epsilon_a = m^2 G / \rho^3$, which is related to the parameter F in the spin-1/2 Bose-Hubbard model Eq. (1) through $F = 2a^3 \rho^3 \epsilon_a J_\uparrow$. Model parameters in the simulations, which are done on a dilute lattice, are chosen such that the period of Bloch oscillations due to the 2π -periodicity of the underlying single-particle lattice dispersion vastly exceeds the simulation time.

We compare the frequency of Bloch oscillations obtained from numerical simulations with the semiclassical result Eq. (64) from Ref. [27] in Fig. 9 (b). The Bloch oscillation frequency ω_b grows with increasing force ϵ_a as one would expect, since the force drives the momentum increase of the impurity. The results we obtain are significantly renormalized from the semiclassical prediction, suggesting higher order interaction effects are playing an important role. We can rule out quantum flutter as being the culprit for the oscillations, since the energy scales are completely different. Note that the Bloch oscillations around the drift velocity are strongly damped and do even exist if the impurity exceeds the sound velocity of the background gas, see Fig. 9 (a), which is not captured in the semiclassical approach of [27]. Reducing the background gas interaction from the TG regime $\gamma_{bg} = \infty$ to $\gamma_{bg} = 5$ does not significantly change the oscillation frequency, Fig. 9 (b), whereas the drift velocity increases, Fig. 9 (a).

For diffusive impurity dynamics the drift velocity is linear proportional to the force $v_d = \mu F$, where μ is the mobility of the impurity, which is shown in Fig. 9 (c) along with predictions from [27]. In contrast to the semiclassical predictions of Ref. [27], the mobility extracted from the numerical simulations is not independent of the force

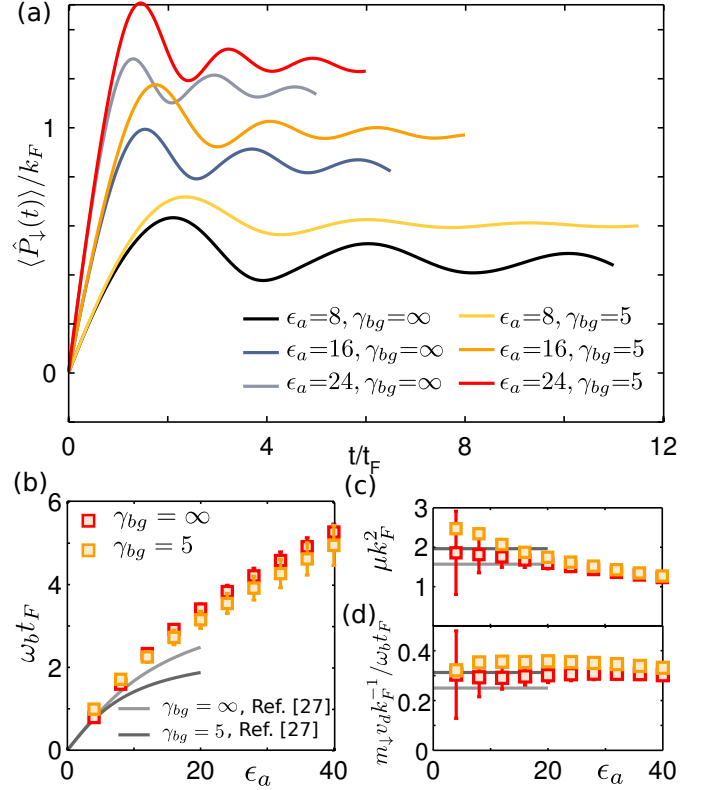


FIG. 9. **Bloch Oscillations:** (Color online) The impurity is accelerated by a constant force ϵ_a . After an initial free acceleration the impurity momentum saturates at the drift velocity around which it oscillates. (a) shows $\langle P_\downarrow(t) \rangle$ for $\gamma = 12$, background gas interactions $\gamma_{bg} = \infty$ and $\gamma_{bg} = 5$, and $\epsilon_a = \{8, 16, 24\}$, respectively, see legend. (b) compares the numerically extracted oscillation frequency ω_b , (c) the mobility μ , and (d) the ratio of the drift velocity v_d and the oscillation frequency ω_b , with the results obtained from a semiclassical analysis, which is valid up to $\epsilon_a \sim 20$ [27].

ϵ_a . In contrast, the ratio of the drift velocity v_d and the Bloch oscillation frequency ω_b , which in the semiclassical analysis is proportional to the mobility, is approximately constant over a very large range of driving ϵ_a also when full quantum mechanical fluctuations are taken into account (d).

In Fig. 10 (a), we compare the expected position of the impurity for both freely accelerated atoms $\gamma = 0$ which follow a parabolic curve and impurities interacting with the background gas with strength $\gamma = 12$. Initially, the trajectories of the two cases cannot be distinguished. However, with increasing time the $\gamma = 12$ trajectory departs from the initial parabolic behavior and develops a linear trend, reflecting that the drift velocity v_d is reached. A renormalization of the impurity trajectory with interactions has also been found in experiments [1], where an imbalanced gas with interaction $\gamma = 7$ has been created, the impurity accelerated with $\epsilon_a = 67$, and its trajectory has been measured up to $\sim 2t_F$. In Fig. 10 (b)

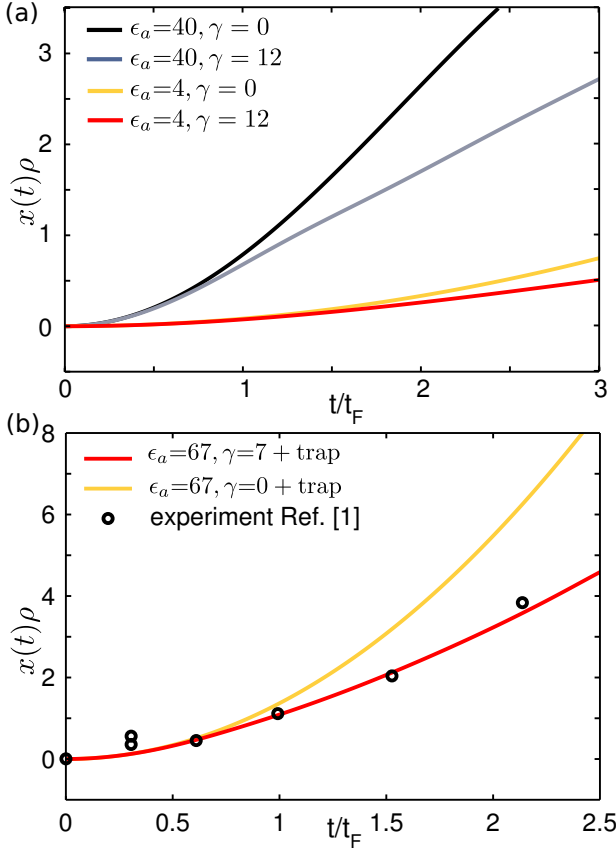


FIG. 10. **Impurity trajectories:** (Color online) Trajectories of the impurity which is driven by a constant force. **(a)** compares the impurity trajectories for finite interactions $\gamma = 12$ to free fall $\gamma = 0$ for different values of the acceleration $\epsilon_a = 4$ and 40. **(b)** compares without any adjustable parameters with the data from experiments [1], where we included the points that correspond to the impurity still being immersed in the background gas, as discussed in Fig. 3 of [1]. In the numerical simulations we fully treat both the interactions and the harmonic confinement.

we compare theory and experiment without adjustable parameters, and find that they are quantitatively compatible. Our calculations fully include both the harmonic trap potential, the interactions γ and $\gamma_{bg} = \infty$, as well as driving force ϵ_a . Note that the trajectory of a free particle in a harmonic trap follows a cosine whose period in the case of the experiment [1] is however much larger than the observed time scales, see Fig. 10 (b), yellow (light shaded) curve.

The constant force acting on the impurity gradually drives it along the ground state dispersion while continuously emitting phonons at the speed of sound u_s [27]—a process which heats the background gas. The power

$$\mathcal{P}_\uparrow = \frac{d}{dt} \langle H_\uparrow(t) \rangle$$

dissipated into the background gas is shown in Fig. 11. At short times \mathcal{P}_\uparrow grows quickly but when the impurity

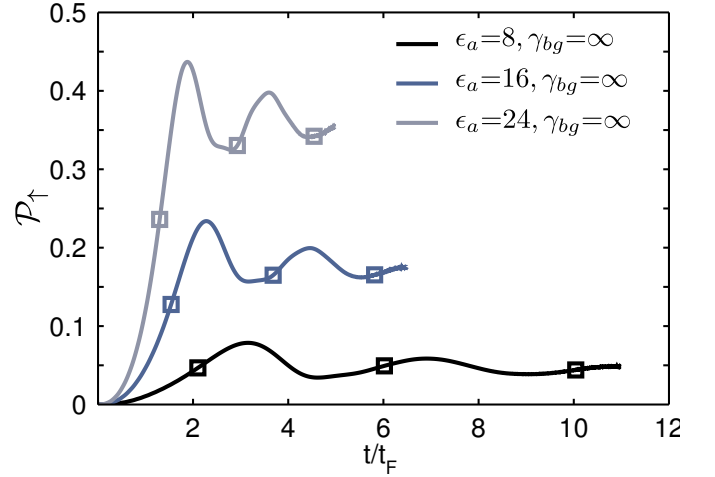


FIG. 11. **Dissipated power:** (Color online) The power \mathcal{P}_\uparrow dissipated in the background gas due to the continuous emission of phonons increases strongly at short times. When the impurity reaches its drift velocity \mathcal{P}_\uparrow reaches a plateau around which it oscillates, providing another signature of Bloch oscillations. Times at which the impurity momentum has a local maximum are indicated by squares. The maxima in \mathcal{P}_\uparrow thus appear at slightly later times than the maxima in the impurity momentum, indicating a retardation effect of the bath.

reaches its drift velocity \mathcal{P}_\uparrow reaches a plateau (in classical systems the constant average heating rate would correspond to Joule heating) around which it oscillates. These oscillations are a further manifestation of Bloch oscillations. The squares highlight the times when the maxima in the impurity momentum $\langle \hat{P}_\downarrow(t) \rangle$ appear. \mathcal{P}_\uparrow shows maxima at the same frequency as those in $\langle \hat{P}_\downarrow(t) \rangle$, however they are lag behind in time.

In addition to the heating of the background gas, the picture of the continuous phonon emission can be directly confirmed by the dynamical density-density correlation function $G_{\downarrow\downarrow}(x, t)$ [Eq. (12)], see Fig. 12, which looks at the density of the background liquid with respect to the impurity position. We find that the significant features occur within a spacetime cone whose apex is at the impurity position at $t = 0$, and which is bounded by the speed of the sound u_s of the background gas (indicated by the dashed lines in Fig. 12, center column). Within the cone, in the forward direction, i.e., the direction in which the impurity is accelerated, the density is increased, while in the backwards direction it is decreased. Thus the impurity is constantly emitting particles and holes symmetrically at the speed of sound u_s around its position. In the TG limit $\gamma_{bg} = \infty$ the speed of sound u_s is given by the Fermi velocity v_F while for $\gamma_{bg} = 5$ it is renormalized to $u_s \sim 0.8v_F$ [22]. The different values of the speed of sound u_s are directly apparent in the different angles of the cones.

The dynamics of $G_{\downarrow\uparrow}(x, t)$ reveals further details of the constantly accelerated impurities: Due to the re-

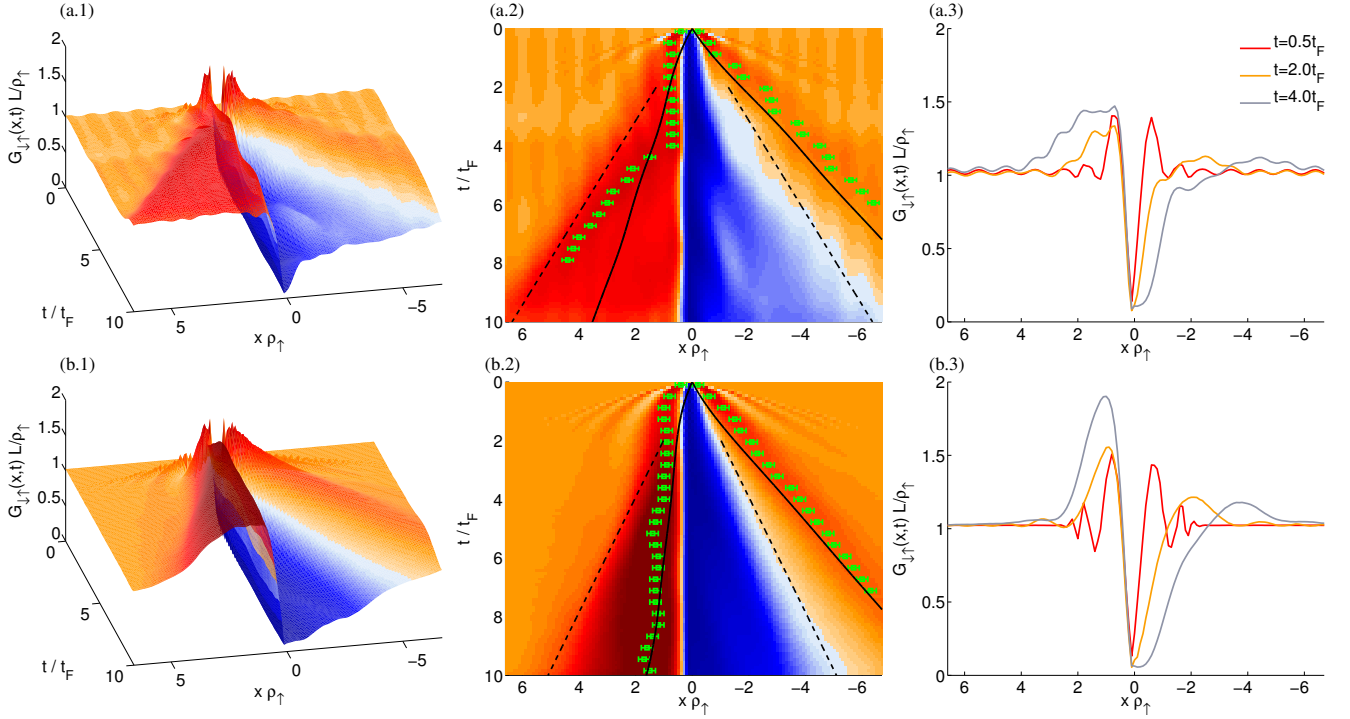


FIG. 12. **Background density for an impurity in gravity.** (Color online) Time evolution of the correlation function $G_{\uparrow\downarrow}(x,t) = \langle \rho_{\downarrow}(0,t) \rho_{\uparrow}(x,t) \rangle$, which represents the density of the background gas around the impurity, for $\gamma = 12$, a finite external force $\epsilon_a = 8$, and background interaction $\gamma_{bg} = \infty$, upper row, and $\gamma_{bg} = 5$, lower row. The other system parameters are chosen as in Fig. 4. The left column shows a perspective view on $G_{\uparrow\downarrow}(x,t)$, the center column a top view, and the right column cuts through $G_{\uparrow\downarrow}(x,t)$ at constant times. The main effect of the impurity on the background density is concentrated around a cone whose demarcations are the dashed lines with slopes given by the speed of sound u_s . In the forward direction (the same direction as the acceleration), the density is increased, while behind the impurity the density is depleted. If we assume that as the impurity creates a correlation hole it emits sound wave packets in the forward and backward directions at $t=0$ at the speed of sound u_s , see shortest times in the right column, then since it is moving with an expected velocity $v(t) = \langle \hat{P}_{\downarrow}(t) \rangle / m_{\downarrow}$, the position of the wave packets at time t will be $\int_0^t dt' (\pm u_s - v(t'))$, where the plus (minus) sign corresponds to the forward (backward) direction. These lines are indicated in black. In green we highlight the maximum of $G_{\uparrow\downarrow}(x,t)$ for $x > 0$, and the same for $x < 0$. In backward direction the green points and black lines almost coincide. In the forward direction the emitted wave packet vanishes in the subsequently emitted flood of phonons. These signatures should be detectable experimentally when measuring the background density with respect to the impurity position.

pulsive interactions, at short times a correlation hole is formed around the impurity and excess particles of the background gas are emitted almost symmetrically both in forward and in backward direction at the speed of sound u_s , see $t = 0.5t_F$ curve in the right column of Fig. 12. The impurity is accelerating, thus its velocity $v(t) = \langle \hat{P}_{\downarrow}(t) \rangle / m_{\downarrow}$ is changing over time. In its frame, therefore, the wave packets will be centered around $\int_0^t dt' (\pm u_s - v(t'))$, the plus (minus) sign corresponding to the wave packet emitted in the forward (backward) direction. In Fig. 12 the lines following this argument are highlighted in black. In the backward direction they coincide with the maximum of the emitted wave packets highlighted in green, where we present the case of a fermionic background (top row) and a background with finite interactions (bottom row). In the forward direction the initially emitted wave packet is overshadowed by the subsequent emission of phonons. These features

could be measured in a cold atom realization by imaging the impurity and the background cloud, averaging over several realizations and measuring position with respect to the impurity position.

As discussed in the previous paragraphs, in the long time limit $t \gtrsim 2t_F$ the impurity reaches the drift velocity around which it weakly oscillates. Therefore the impurity frame is approximately constant provided $t \gtrsim 2t_F$, essentially allowing in that regime for the symmetric shape of the cone, which reflects the emitted particle-hole pairs, and for the approximately linear propagation of the wave packets created while the correlation hole is formed.

V. CONCLUSIONS

In summary, we have studied two types of oscillations arising from the nonequilibrium dynamics of an impu-

rity coupled to a one-dimensional quantum liquid. In the first case, the impurity is given an initial momentum from which it only sheds a part to the background liquid. Further the impurity momentum undergoes coherent oscillations in time provided that the initial momentum is of the order of or larger than the Fermi momentum. In the second case, the impurity is initially at rest but subject to a constant force, which accelerates the impurity up to a finite velocity around which it performs Bloch oscillations arising from the $2k_F$ periodicity of the ground state branch. The results obtained in both cases are independent of whether the system is integrable or not and are robust to changes in the parameters of the system, including a trapping potential, which lends support to the suggestion of seeing signatures of the physical phenomena we describe in a cold atomic setup. Our results are in quantitative agreement and therefore possibly an ex-

planation of experimental results on an impurity driven by a constant force [1].

ACKNOWLEDGMENTS

We are grateful to E. Haller, A. Kamenev, A. Lamacraft, and H.C. Nägerl for fruitful discussions and to M. Ganahl for providing his MPS code [45]. The authors acknowledge support from Harvard-MIT CUA, the NSF Grants No. DMR-07-05472, the DARPA OLE program, AFOSR Quantum Simulation MURI, the Austrian Marshall Plan Foundation and the Austrian Science Fund (FWF) Project No. J 3361-N20, as well as the Swiss National Science Foundation through the grant PA00P2.126228. Calculations have been performed on the Vienna Scientific Cluster (VSC II).

-
- [1] S. Palzer, C. Zipkes, C. Sias, and M. Köhl, *Phys. Rev. Lett.* **103**, 150601 (2009).
 - [2] C. Weitenberg, M. Endres, J. F. Sherson, M. Cheneau, P. Schau, T. Fukuhara, I. Bloch, and S. Kuhr, *Nature* **471**, 319 (2011).
 - [3] J. Simon, W. S. Bakr, R. Ma, M. E. Tai, P. M. Preiss, and M. Greiner, *Nature* **472**, 307 (2011).
 - [4] T. Fukuhara, A. Kantian, M. Endres, M. Cheneau, P. Schauß, S. Hild, D. Bellem, U. Schollwöck, T. Giamarchi, C. Gross, I. Bloch, and S. Kuhr, *Nat. Phys.* (2013), 10.1038/nphys2561.
 - [5] J. Catani, G. Lamporesi, D. Naik, M. Gring, M. Inguscio, F. Minardi, A. Kantian, and T. Giamarchi, *Phys. Rev. A* **85**, 023623 (2012).
 - [6] A. O. Gogolin, A. A. Nersisyan, and A. M. Tsvelik, *Bosonization And Strongly Correlated Systems* (Cambridge University Press, Cambridge, UK, 2004).
 - [7] T. Giamarchi, *Quantum Physics in One Dimension* (Oxford University Press, USA, 2004).
 - [8] J. B. McGuire, *J. Math. Phys.* **6**, 432 (1965).
 - [9] J. B. McGuire, *J. Math. Phys.* **7**, 123 (1966).
 - [10] J. N. Fuchs, D. M. Gangardt, T. Keilmann, and G. V. Shlyapnikov, *Phys. Rev. Lett.* **95**, 150402 (2005).
 - [11] O. Giraud and R. Combescot, *Phys. Rev. A* **79**, 043615 (2009).
 - [12] H. Castella and X. Zotos, *Phys. Rev. B* **47**, 16186 (1993).
 - [13] H. Castella, *Phys. Rev. B* **54**, 17422 (1996).
 - [14] M. B. Zvonarev, V. V. Cheianov, and T. Giamarchi, *Phys. Rev. Lett.* **99**, 240404 (2007).
 - [15] S. Akhanev and Y. Tserkovnyak, *Phys. Rev. B* **76**, 140408(R) (2007).
 - [16] T. Ogawa, A. Furusaki, and N. Nagaosa, *Phys. Rev. Lett.* **68**, 3638 (1992).
 - [17] P. Nozières, *Journal de Physique I* **4**, 1275 (1994).
 - [18] Y. Tsukamoto, T. Fujii, and N. Kawakami, *Phys. Rev. B* **58**, 3633 (1998).
 - [19] K. A. Matveev and A. Furusaki, *Phys. Rev. Lett.* **101**, 170403 (2008).
 - [20] A. Kamenev and L. Glazman, *Phys. Rev. A* **80**, 011603(R) (2009).
 - [21] M. B. Zvonarev, V. V. Cheianov, and T. Giamarchi, *Phys. Rev. Lett.* **103**, 110401 (2009).
 - [22] M. B. Zvonarev, V. V. Cheianov, and T. Giamarchi, *Phys. Rev. B* **80**, 201102 (2009).
 - [23] A. H. Castro Neto and M. P. A. Fisher, *Phys. Rev. B* **53**, 9713 (1996).
 - [24] D. M. Gangardt and A. Kamenev, *Phys. Rev. Lett.* **102**, 070402 (2009).
 - [25] T. H. Johnson, S. R. Clark, M. Bruderer, and D. Jaksch, *Phys. Rev. A* **84**, 023617 (2011).
 - [26] M. Schechter, D. M. Gangardt, A. Kamenev, and A. Lamacraft, *Phys. Rev. Lett.* **108**, 207001 (2012).
 - [27] M. Schechter, D. M. Gangardt, and A. Kamenev, *Ann. Phys.* **327**, 639 (2012).
 - [28] J. Bonart and L. F. Cugliandolo, *Phys. Rev. A* **86**, 023636 (2012).
 - [29] F. Massel, A. Kantian, A. J. Daley, T. Giamarchi, and P. Törmä, *arXiv:1210.4270* (2012).
 - [30] S. Peotta, D. Rossini, M. Polini, F. Minardi, and R. Fazio, *Phys. Rev. Lett.* **110**, 015302 (2013).
 - [31] C. J. M. Mathy, M. B. Zvonarev, and E. Demler, *Nat. Phys.* **8**, 881 (2012).
 - [32] V. E. Korepin, N. M. Bogoliubov, and A. G. Izergin, *Quantum Inverse Scattering Method and Correlation Functions* (Cambridge University Press, Cambridge, 1993).
 - [33] B. Sutherland, *Beautiful Models* (World Scientific, Singapore, 2004).
 - [34] T. Kinoshita, T. Wenger, and D. S. Weiss, *Nature* **440**, 900 (2006).
 - [35] M. Rigol, *Phys. Rev. A* **80**, 053607 (2009).
 - [36] M. Colomé-Tatché and D. S. Petrov, *Phys. Rev. Lett.* **106**, 125302 (2011).
 - [37] G. Vidal, *Phys. Rev. Lett.* **91**, 147902 (2003).
 - [38] G. Vidal, *Phys. Rev. Lett.* **93**, 040502 (2004).
 - [39] S. R. White, *Phys. Rev. Lett.* **69**, 2863 (1992).
 - [40] U. Schollwöck, *Rev. Mod. Phys.* **77**, 259 (2005).
 - [41] F. H. L. Essler, H. Frahm, F. Göhmann, A. Klümper, and V. E. Korepin, *The One-Dimensional Hubbard Model* (Cambridge University Press, Cambridge, 2005).
 - [42] C. N. Yang, *Phys. Rev. Lett.* **19**, 1312 (1967).
 - [43] M. Gaudin, *La fonction d'onde de Bethe* (Masson, Paris, New York, 1983).

- [44] E. H. Lieb, [Phys. Rev. **130**, 1616 \(1963\)](#).
- [45] M. Ganahl, E. Rabel, F. H. L. Essler, and H. G. Evertz, [Phys. Rev. Lett. **108**, 077206 \(2012\)](#).